

The effect of receptor interaction on the bacterial chemotactic adaptation rate

Shujian Ren*, Chi Zhang* , and Rongjing Zhang 

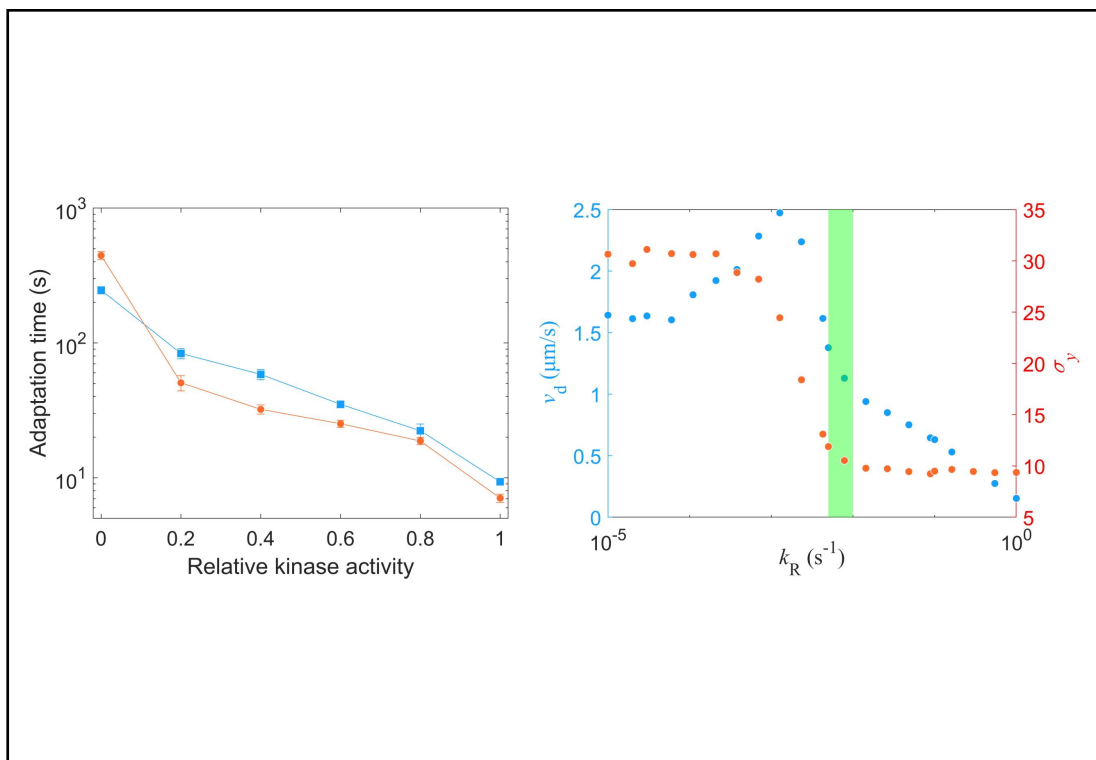
Hefei National Research Center for Physical Sciences at the Microscale, and Department of Physics, University of Science and Technology of China, Hefei 230026, China

* These authors contributed equally to this work

 Correspondence: Chi Zhang, E-mail: zhchi@ustc.edu.cn; Rongjing Zhang, E-mail: rjzhang@ustc.edu.cn

© 2023 The Author(s). This is an open access article under the CC BY-NC-ND 4.0 license (<http://creativecommons.org/licenses/by-nc-nd/4.0/>).

Graphical abstract





The interaction of chemoreceptors in *Escherichia coli* influences the rate of adaptation and enhances bacterial chemotaxis.

Public summary

- The wild-type *Escherichia coli* (*E. coli*) strain exhibits faster adaptation than the mutant expressing only one type of receptors, when subjected to the same concentration of saturated stimulus.
- The wild-type strain exhibits slower adaptation than the mutant under unsaturated stimuli that induce the same magnitude of response, and this is independent of the level of receptor expression.
- The interaction between different types of receptors in *E. coli* can effectively enhance chemotaxis under a stable spatial gradient of attractants, while simultaneously ensuring minimum noise in the cell position distribution.

The effect of receptor interaction on the bacterial chemotactic adaptation rate

Shujian Ren*, Chi Zhang* , and Rongjing Zhang 

Hefei National Research Center for Physical Sciences at the Microscale, and Department of Physics, University of Science and Technology of China, Hefei 230026, China

* These authors contributed equally to this work

 Correspondence: Chi Zhang, E-mail: zhchi@ustc.edu.cn; Rongjing Zhang, E-mail: rjzhang@ustc.edu.cn

© 2023 The Author(s). This is an open access article under the CC BY-NC-ND 4.0 license (<http://creativecommons.org/licenses/by-nc-nd/4.0/>).



Cite This: JUSTC, 2023, 53(7): 0703 (9pp)



Read Online

Abstract: Different receptors have evolved in organisms to sense different stimuli in their surroundings. The interaction among the receptors can significantly increase sensory sensitivity and adaptation precision. To study the influence of interaction among different types of chemoreceptors on the adaptation rate in the bacterial chemotaxis signaling network, we systematically compared the adaptation time between the wild-type strain expressing mixed types of receptors and the mutant strain expressing only Tar receptors (namely, the Tar-only strain) under stepwise addition of different concentrations of L-aspartate using FRET (Förster resonance energy transfer) and bead assays. We find that the wild type exhibits faster adaptation than the mutant under the same concentration of saturated stimulus. In contrast, the wild type exhibits slower adaptation than the mutant under unsaturated stimuli that induce the same magnitude of response, and this is independent of the level of receptor expression. The same result is obtained for the network relaxation time by monitoring the steady-state rotational signal of the flagellar motors. By simulating bacterial chemotaxis with different adaptation rates in a stable gradient of chemoattractants, we confirm that the interaction of different types of receptors can effectively promote chemotaxis of *Escherichia coli* under a stable spatial gradient of attractants while ensuring minimum noise in the cell position distribution.

Keywords: chemoreceptor; interaction; adaptation rate; bacterial chemotaxis

CLC number: Q6-3

Document code: A

1 Introduction

Organisms can sense and adapt to many signals in the environment. A variety of specific receptors have evolved for different kinds of stimuli^[1-3]. In *Escherichia coli* (*E. coli*), there are five different types of transmembrane chemoreceptors, among which Tar and Tsr are the two most abundant^[4,5]. Structural studies have shown that these receptors form regular arrays on the cell membrane (especially the cell poles) with heterotrimers of homodimers with the help of the kinase CheA and the scaffold protein CheW^[6-8]. The autophosphorylation of CheA is suppressed (enhanced) when the attractant (repellent) ligands bind to the receptors, which in turn regulates the phosphorylation level of the response regulator CheY^[9,10]. Phosphorylated CheY, called CheY-P, binds to the cytoplasmic domain of the flagellar motors and modulates their rotational direction and cell swimming state accordingly^[11-13]. Previous experimental and theoretical studies have confirmed the existence of strong interactions among chemoreceptors^[14-17]. This leads to large signal amplification and high sensitivity in bacterial chemotaxis^[16,18]. Moreover, interactions among different types of receptors can amplify the response of mixed clusters to specific stimuli^[19,20].

In addition to the effect on signal amplification, receptor interaction plays an important role in adaptation in bacterial

chemotaxis^[21,22]. Chemotaxis adaptation is accomplished via covalent modification of receptors by CheR and CheB proteins, which are responsible for methylating and demethylating receptors, respectively^[23,24]. Measurements in vitro showed that both tethered CheR and CheB can act on an assistance neighborhood of five to seven nearby receptors, which is necessary for precise adaptation in a model of receptor clusters composed of different types of receptors^[25-28].

Much work has focused on the significance of receptor interaction in sensory amplification and adaptation in bacterial chemotaxis, but research related to the latter has mainly focused on the accuracy of adaptation^[29-33], while the effect of receptor interaction on the adaptation rate remains unclear. The work of Tu et al.^[32,33] demonstrated that the adaptive behavior of bacteria is dissipative and determined the relationship between energy dissipation, adaptation rate, and adaptation accuracy. Since the interaction of different types of receptors has a significant effect on the accuracy of bacterial adaptation, it should also affect the adaptation rate, which we seek to investigate in this study.

Here, we systematically compare the adaptation time between the wild-type strain expressing mixed types of receptors and the mutant strain expressing only Tar receptors (namely, the Tar-only strain) under stepwise addition of different

concentrations of L-aspartate (a kind of attractant sensed by Tar receptors) by FRET and bead assays. We find that the wild-type strain spends less time to finish adaptation to the same saturated concentration of attractant (10 $\mu\text{mol/L}$ L-aspartate); that is, it recovers faster when encountering a saturated stimulus. In contrast, it performs slower adaptation (longer adaptation time) than the Tar-only strain when subjected to stepwise additions of unsaturated concentrations of L-aspartate that induce the same relative changes in receptor-kinase activity. By adjusting the expression level of the Tar receptors in the Tar-only strain, we confirm that this difference in adaptation time does not result from the different expression levels of receptors. We also compare the adaptation time when the concentration of stimulus was zero (that is, the network relaxation time) by monitoring the flagellar motor rotation of unstimulated cells in a steady state. The wild type also exhibits a longer adaptation time than the mutant in this extreme case. To elucidate the effect of adaptation time on bacterial chemotactic behavior, we perform stochastic simulations of bacterial chemotaxis in an exponential concentration gradient of MeAsp (the unmetabolized analog of L-aspartate). We find that longer adaptation times lead to greater drift velocities. Thus, the interaction of different types of receptors can effectively promote chemotaxis of *E. coli* under a stable spatial gradient of attractant. At the same time, it can help the bacterium recover faster when encountering a saturated stimulus.

2 Results

2.1 Adaptation to a saturated concentration of L-aspartate

The phosphorylation of the response regulator CheY by the kinase CheA and dephosphorylation of CheY-P by CheZ bring the concentration of CheY-P into balance in living cells. Thus, we can follow the receptor-kinase activity (the probability that the receptor is activated) in vivo by monitoring the FRET signal between CheY and its phosphatase CheZ, which were fused with eYFP and eCFP, respectively^[34,35].

To study the effect of the interaction between different types of chemoreceptors on bacterial adaptation, we measured the response of receptor-kinase activity to stepwise addition of the same saturated concentration of L-aspartate for both the wild-type strain (HCB1288-pVS88) and the mutant expressing only Tar receptors (HCB1414-pLC113-pVS88). We used 1 $\mu\text{mol/L}$ sodium salicylate to induce the expression of Tar receptors at a wild-type level for the mutant^[36].

The FRET measurements were performed following a similar procedure described previously^[37]. A typical FRET response of a bacterial population to stepwise addition and removal of 10 $\mu\text{mol/L}$ L-aspartate is shown in Fig. 1a. The stimulus was added at $t = 120$ s and removed at $t = 600$ s. The source of different responses between addition and removal stimulus is the phosphorylation of CheB by CheA, which can greatly increase the rate of receptor demethylation^[23]. The adaptation time is defined as denoted in Fig. 1a. We calculated the adaptation time in each measurement for both strains. As shown in Fig. 1b, the adaptation times were (246 ± 15) s and

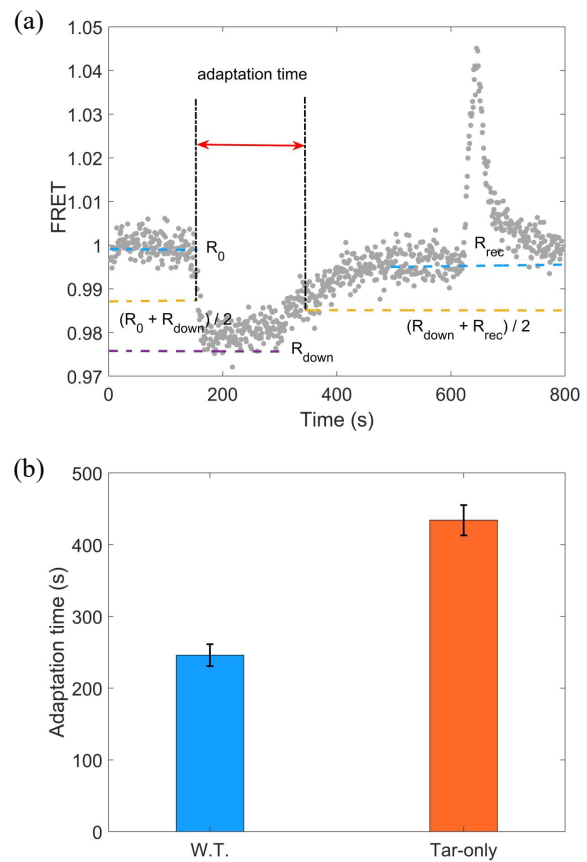


Fig. 1. (a) A typical trace of the step response to 10 $\mu\text{mol/L}$ L-aspartate. The stimulus was added at $t = 120$ s and removed at $t = 600$ s. The FRET value was defined as the intensity ratio of the YFP to CFP channel. The definition of the adaptation time is indicated. (b) The adaptation time to 10 $\mu\text{mol/L}$ L-aspartate for the wild-type (W.T.) strain (HCB1288-pVS88) and the Tar-only strain (HCB1414-pLC113-pVS88). The errors denote the standard deviations.

(434 ± 21) s for the wild-type (W.T.) and Tar-only strains, respectively. The errors denote standard deviations. Thus, the wild type with mixed types of receptors adapted faster than the Tar-only strain to the same saturated concentration of L-aspartate.

2.2 Adaptation to unsaturated concentrations of L-aspartate

We find that wild-type *E. coli* adapted faster than the mutant to the same saturating concentration of 10 $\mu\text{mol/L}$ L-aspartate. During most of the adaptation (or recovery) process when subjected to 10 $\mu\text{mol/L}$ L-aspartate, the receptor-kinase activity was suppressed to zero. To compare the adaptation when the receptor-kinase activity was not suppressed to zero, we sought to measure the adaptation process when subjected to unsaturated concentrations of L-aspartate.

As the magnitude of kinase activity response to the same unsaturated concentrations of L-aspartate was different for the wild-type and Tar-only strains, we first measured the dose-response curve for each of them. An example of the dose-response measurement is shown in Fig. 2a. Then, the relation between the responses (horizontal red solid lines) and the concentrations of L-aspartate was extracted.

The dose–response curves of relative kinase activity to L-aspartate concentration we measured for the wild-type and Tar-only strains are shown in Fig. 2b. The Hill function was used to fit each of them. The fitted Hill coefficients were 1.84 ± 0.17 and 1.97 ± 0.20 for the wild-type and Tar-only strains, respectively. The concentrations for half-maximal response ($K_{0.5}$) obtained from the fits were $(1.93 \pm 0.11) \mu\text{mol/L}$ and $(0.64 \pm 0.04) \mu\text{mol/L}$ for the wild-type and Tar-only strains, respectively. The error denotes the standard deviation.

We also fit our data with the all-or-none Monod-Wyman-Changeux (MWC) model of receptor cooperativity to extract the size of the receptor cluster $N^{[38-40]}$:

$$a = \frac{1}{1 + \exp\left(N\left(\alpha(m_0 - m) + \ln \frac{1 + L/K_{\text{off}}}{1 + L/K_{\text{on}}}\right)\right)}, \quad (1)$$

where a is the receptor-kinase activity, m is the methylation level, L is the ligand concentration, and K_{off} and K_{on} are the

ligand dissociation constants for the inactive and active receptors, respectively. We used $\alpha = 1.7$, $m_0 = 1.0$, $K_{\text{off}} = 1.7 \mu\text{mol/L}$, and $K_{\text{on}} = 12 \mu\text{mol/L}$ (for Asp) from previous works^[41,42]. According to the dose–response curves, the size of receptor cluster N was extracted to be 4.6 ± 1.0 and 8.9 ± 1.9 for the wild-type and Tar-only strains, respectively. Thus, the Tar receptors of the mutant exhibit higher cooperativity despite being expressed at the same level as the wild type.

To carry out a direct comparison, we sought to measure the adaptation times for the wild-type and Tar-only strains when their receptor-kinase activity was lowered to the same level relative to the pre-stimulus activity by stepwise addition of specific unsaturated concentrations of L-aspartate. As marked in the dose–response curve in Fig. 2b, the concentrations of L-aspartate that induced relative kinase activity responses of 0.2, 0.4, 0.6, and 0.8 for each strain were selected for the step response measurements, as shown in Fig. 1a. For a more meaningful comparison, we plotted the adaptation time against the relative kinase activity instead of the aspartate concentration, and the relationship between adaptation time

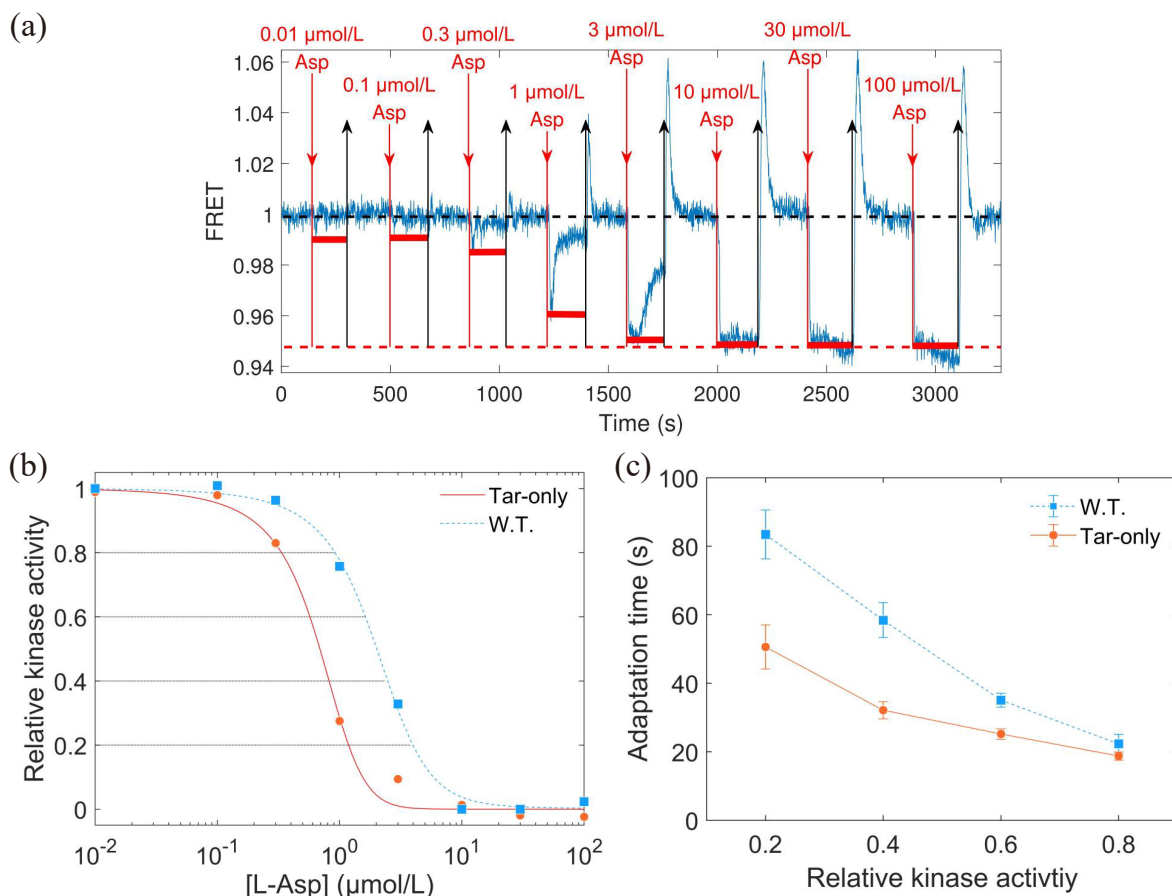


Fig. 2. (a) The dose–response measurement to L-aspartate. The blue line is the FRET signal. The red downward arrows denote the time when the stimulus was added, while the black upward arrows indicate the time when the stimulus was removed. The black and red dashed lines represent the pre-stimulus and saturated FRET values, respectively. (b) The dose–response curve of relative kinase activity (relative to the pre-stimulus value) to the concentration of L-aspartate for both strains. The relative kinase activity was obtained by rescaling the FRET values of 1 (the pre-stimulus value, black dashed line in (a)) to 0.95 (the value after adding a saturated concentration of stimulus, red dashed line in (a)) to the range between 1 and 0. The blue and red lines are the results fitted with the MWC model for the wild-type and mutant strains, respectively. The gray lines indicate the values of relative kinase activity used in the step-response measurements. (c) The relation between adaptation time and relative kinase activity response. The errors denote standard deviations.

and relative kinase activity is shown in Fig. 2c. The errors denote standard deviations. In contrast to the result of stimulation by saturated concentration, the wild-type strain showed slower adaptation to unsaturated concentrations of L-aspartate than the mutant.

2.3 Tar expression levels do not affect the adaptation time of the mutant to unsaturated concentrations of L-aspartate

To study the effect of the expression level of Tar receptors on adaptation time, we tried to change the level of receptor expression by varying the concentration of inducers. We used 0.5 $\mu\text{mol/L}$ sodium salicylate (half-concentration inducer) to induce the expression of Tar receptors for the Tar-only strain instead of 1 $\mu\text{mol/L}$ (wild-type level). The comparison of dose–response curves for the two concentrations of inducer is shown in Fig. 3a. We also fit the data with the Hill function and Eq. (1), and the half-concentration inducer leads to $H = 2.26 \pm 0.15$, $K_{0.5} = (1.24 \pm 0.04) \mu\text{mol/L}$, and the receptor cluster size $N = 6.4 \pm 0.8$. Thus, reducing the level of receptor expression decreases the cooperativity among them and the sensitivity of response to stimuli.

We also measured the adaptation time for relative kinase activity responses of 0.2, 0.4, 0.6, and 0.8. As shown in

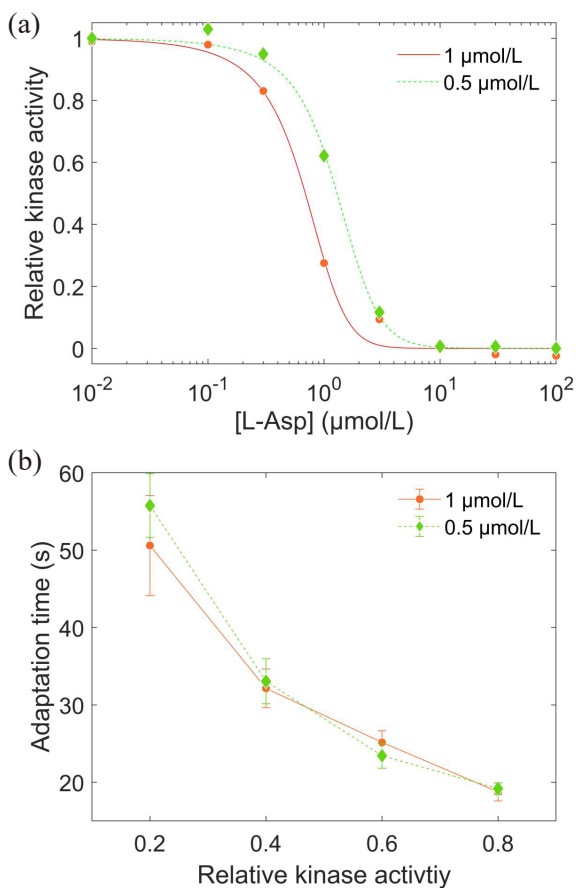


Fig. 3. (a) The dose–response curves of the Tar-only strain under 1 $\mu\text{mol/L}$ (red dots, wild-type level) and 0.5 $\mu\text{mol/L}$ (green diamonds) inducer (sodium salicylate). The smooth lines are the results fitted with the MWC model. (b) The relation between adaptation time and relative kinase activity response. The errors denote standard deviations.

Fig. 3b, there was no difference in adaptation time between the two expression levels of Tar receptors. Thus, the expression levels of receptors do not affect the adaptation time to unsaturated concentrations of L-aspartate, indicating that the adaptation enzymes CheR and CheB are probably not working at saturation under these situations.

2.4 The unstimulated wild-type cells exhibited a longer relaxation time

It is difficult to measure the adaptation time under a very low concentration of L-aspartate by the method above because of the noisy chemotactic signal. The good news is that the adaptation time under very low stimulation is equivalent to the chemotaxis network relaxation time, which can be obtained from the spontaneous fluctuations of chemotaxis output for unstimulated cells in a steady state^[43,44]. Considering that fluctuations in receptor-kinase activity are ultimately reflected in the rotational direction of the flagellar motors, we chose the motor rotational state as an indicator of the chemotaxis output and measured the relaxation time using a procedure similar to that described previously^[45].

We monitored motor rotation using a bead assay. As shown in Fig. 4a, a 1 μm -diameter latex bead was attached to a truncated sticky flagellar stub. The trajectories of rotating beads were recorded with a high-speed camera equipped on a phase-contrast microscope. The traces of rotation speed can then be calculated from the trajectories. An example is shown in Fig. 4b. The positive and negative values of speeds represent the CCW- and CW-rotational states of the motor, respectively.

We monitored the motor rotation of the wild-type strain (JY26-pKAF131) and the mutant expressing only Tar receptors (CZ1-pLC113-pFD313) for 18 min. As shown in Fig. 4c, the wild-type and mutant strains exhibited the same CW bias distribution with average CW bias = 0.14 ± 0.08 and 0.15 ± 0.09 , respectively. This indicates that they exhibit similar unstimulated kinase activity. 97 motors were measured for wild-type cells and 30 for mutant cells. We calculated the correlation time, which is equivalent to the relaxation or adaptation time, for both strains (see Section 4 for details). The equivalence of the pre-stimulus correlation time and the adaptation time to a weak stimulus is a consequence of the linear approximation for the chemotaxis system under weak stimuli^[44]. As shown in Fig. 4d, the adaptation times were $(9.3 \pm 0.4) \text{ s}$ and $(7.1 \pm 0.5) \text{ s}$ for the wild type and the mutant, respectively. Similar to the adaptation measured by FRET under the unsaturated concentration of L-aspartate, the wild-type strain also exhibits a slower adaptation than the mutant at zero-concentration stimulus.

2.5 Simulation of bacterial chemotactic swimming with different adaptation rates

Here, we found different adaptation rates between the wild type and the Tar-only strain, as summarized in Fig. 5a. To determine the physiological significance of these different adaptation rates on bacterial chemotaxis, we used the SPEC model^[39] to simulate the chemotaxis of *E. coli* with different adaptation rates in a stationary exponential concentration gradient of α -methyl-aspartate (MeAsp, the unmetabolized

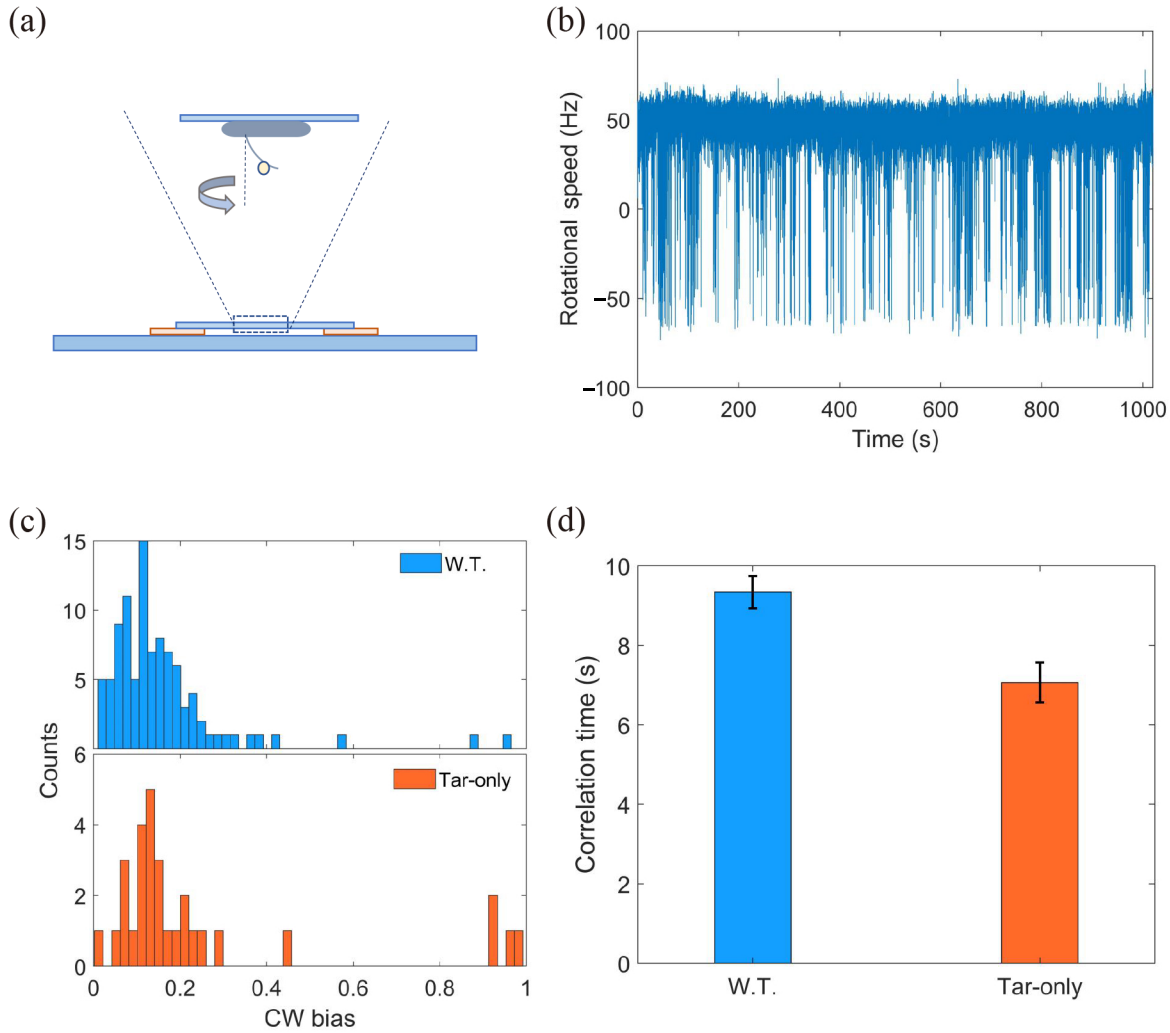


Fig. 4. (a) Schematic diagram of the bead assay for the flagellar motor. (b) A typical trace of the rotational speed (blue line) of individual motors. The positive and negative values of speed denote CCW and CW rotation, respectively. (c) The CW bias distribution for the wild-type and Tar-only strains. (d) The correlation times for both strains.

analog of L-aspartate).

Cells were treated as self-propelled particles whose motion states could be either swimming smoothly (run) or stopping and reorienting (tumble) in our simulation. The motion states were determined by the intracellular chemotactic signal. The chemotactic signal process can be summarized into two parts: sensing and adaptation^[38], with sensing described by Eq. (1) and adaptation described by

$$\frac{dm}{dt} = k_R(1-a) - k_B a, \quad (2)$$

where a is the receptor-kinase activity, m is the methylation level of receptors, and k_R and k_B represent the methylation and demethylation rate constants, respectively.

The concentration of CheY-P (Y_p) depends on the kinase activity by $Y_p = 7.86a$ and leads to the CW bias (B) of the flagellar motor by^[46]

$$B = \frac{Y_p^{10.3}}{Y_p^{10.3} + 3.1^{10.3}}. \quad (3)$$

The switching rate of cell motion from run to tumble is de-

termined as $B/0.11 \text{ s}^{-1}$, while the switching rate from tumble to run is 5 s^{-1} ^[47].

2000 cells were simulated for 1200 s in an exponential MeAsp concentration profile $L(x) = 91 \exp(x/5000) \mu\text{mol/L}$, where x is in the unit of μm . As shown in Fig. 5b, the mean position of the cell population exhibited a constant chemotactic drift velocity v_d along the gradient. The drift velocity can be obtained by fitting the data with a linear function. We changed the methylation rate constant k_R from 10^{-5} s^{-1} to 1.0 s^{-1} to induce different adaptation rates (the inverse of adaptation time) and kept $k_B = 2k_R$. The relation between v_d and k_R is shown in Fig. 5c. According to our results, a smaller adaptation rate (longer adaptation time) leads to a greater drift velocity in an exponential concentration gradient of attractant. We also calculated the variance of the y position of the cell distribution σ_y . The wild-type strain maintained the minimum noise of the cell position distribution, as shown in Fig. 5c.

3 Conclusions and discussion

Organisms evolve different kinds of receptors to sense different stimuli in the environment. It has been demonstrated that

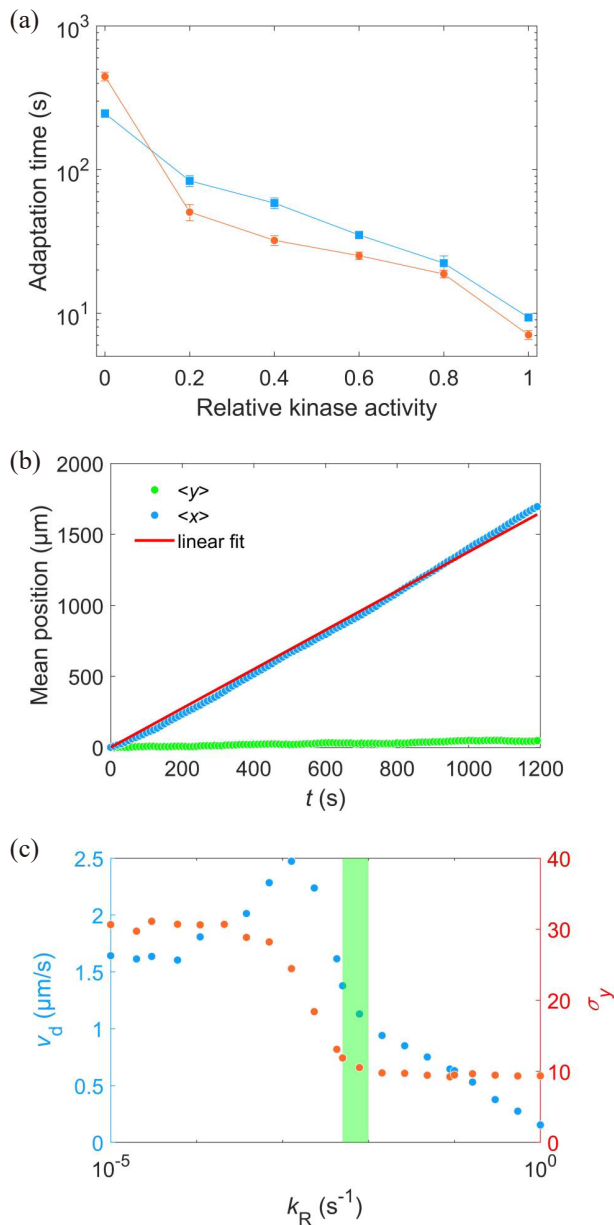


Fig. 5. (a) Comparison of adaptation times between the wild-type (blue squares) and Tar-only strains (red dots) for all concentrations of L-aspartate. The errors denote standard deviations. (b) The change in mean position over time in a gradient of exponential MeAsp concentration profile $L(x) = 91\exp(x/5000)$. The blue dots represent the mean x position. The green squares denote the mean y position. The red line is the linear fit to the blue dots. (c) The effect of adaptation rate on bacterial chemotaxis. Blue and red dots represent the drift velocity in the x direction and the variance of the y positions under different values of k_R . The value of k_R ranges from 0.005 s^{-1} to 0.01 s^{-1} for the wild-type strain, which is marked by the green shaded area.

there are strong interactions between chemoreceptors that have an important effect on the chemotactic behavior of bacteria. Previous studies on the role of receptor interactions in bacterial chemotaxis have focused on signal amplification and the accuracy of adaptation.

In this study, we systematically studied the effect of interactions between different types of receptors on the adaptation rate of *E. coli*. We measured the adaptation time of both the

wild-type strain with mixed types of receptors and the mutant expressing only Tar receptors under different concentrations of L-aspartate via FRET and bead assays. We found that the wild type showed faster adaptation than the mutant under the same saturated concentration of attractant. The adaptation times under the stimulation of $10\text{ }\mu\text{mol/L}$ L-aspartate were $(246\pm 15)\text{ s}$ and $(434\pm 21)\text{ s}$ for the wild type and mutant, respectively.

We also compared the adaptation times to unsaturated L-aspartate concentrations that induced the same degree of kinase activity response for the two strains. The results were different from those obtained under the stimulation of saturated concentrations of L-aspartate. The wild-type strain showed slower adaptation than the mutant. By adjusting the expression level of the Tar receptors, we confirmed that reducing the expression concentration of Tar decreases the cooperativity among them and the sensitivity to stimuli but does not change the adaptation time. Thus, the different adaptation rates between the wild-type strain and the Tar-only strain did not result from the different expression levels of receptors. We also studied the adaptation time when the concentration of stimulus was zero by monitoring flagellar motor rotation at steady states without a stimulus. The wild type also exhibits a longer adaptation time than the mutant in this extreme case. Why does the Tar-only mutant adapt faster than the wild-type strain to unsaturated stimuli? This might be because the mutant exhibits a larger receptor cluster ($N = 4.6\pm 1.0$ and 8.9 ± 1.9 for the wild-type and Tar-only strains, respectively), such that each CheR molecule covers a wider range of receptors (a larger number of assistance neighbors)^[28].

To determine the physiological significance of these different adaptation rates on bacterial chemotaxis, we used the SPEC model to simulate the chemotaxis of *E. coli* with different adaptation rates in a stationary exponential concentration gradient of α -methyl-aspartate. We found that a smaller adaptation rate (a longer adaptation time) leads to a greater drift velocity and a wider distribution of cell location in a steady exponential concentration gradient of attractant, while the adaptation rate of the wild-type cells ensures minimum noise of cell position distribution (Fig. 5c). Therefore, the interaction between different types of chemoreceptors can effectively promote the chemotaxis of *E. coli* under a stable spatial gradient field while ensuring minimum noise of the cell position distribution. At the same time, the faster recovery/adaptation of the wild-type strain to saturated stimuli (compared to the mutant) ensures that it can recover faster when accidentally encountering a strong stimulus in the environment.

4 Materials and methods

4.1 Strains and plasmids

The strains used in this study are derivatives of *E. coli* K12 strain RP437: JY26(Δ fliC), CZ1(Δ fliC tar tsr tap), HCB1288(Δ cheY cheZ), and HCB1414(Δ cheY cheZ tar tsr tap aer). The plasmid pVS88 expresses CheZ-eCFP and CheY-eYFP under an isopropyl- β -D-thiogalactopyranoside (IPTG)-inducible promoter. The plasmid pLC113 expresses Tar receptors under a salicylate-inducible promoter. The

plasmids pKAF131 and pFD313 constitutively express sticky FliC.

HCB1288 transformed with pVS88 and HCB1414 transformed with pVS88 and pLC113 were used to perform FRET experiments. JY26 transformed with pKAF131 and CZ1 transformed with pLC113 and pFD313 were used for bead assays.

4.2 Cell culture

Cells were grown at 33 °C under vigorous shaking (200 r/min) in 10 mL of T-broth (1% (w/v) tryptone and 0.5% (w/v) NaCl) with the appropriate antibiotics (ampicillin (100 µg/mL) and chloramphenicol (50 µg/mL)) and the inducers (0.1 mmol/L IPTG and 1 µmol/L, 0.5 µmol/L sodium salicylate) to an optical density at 600 nm of between 0.45 and 0.5. Then, they were collected by centrifugation (6 min at 3500 g (gravitational acceleration) for the FRET experiment and 2 min at 4000 g for the bead assay), washed twice with 10 mL of motility medium (10 mmol/L potassium phosphate, 0.1 mmol/L EDTA, 1 µmol/L methionine, 10 mmol/L lactic acid (pH 7.0)), and resuspended in 10 mL of this medium. The washed cell suspensions were stored at 4 °C.

4.3 FRET measurements

We followed the receptor-kinase activity *in vivo* by monitoring the FRET signal between CheY-eYFP and CheZ-eCFP using a FRET setup described previously^[36]. The washed cells were kept in a dark box at room temperature (23 °C) for 1–1.5 h to wait for the maturation of the fluorescent proteins. Then, 1 mL of cell suspension was concentrated to 80 µL and injected into the flow cell equipped with a poly-L-lysine-coated cover glass. We used a Nikon Ti-E microscope with a 40× 0.60 NA objective to observe the samples. The YFP and CFP signals were collected by two photon-counting photomultipliers (Hamamatsu, H7421-40PMT). The FRET value was defined as the intensity ratio of YFP to CFP signals. The dose–response and step–response experiments were performed with a constant flow rate of 500 µL/min. Our data were analyzed with a custom script in MATLAB.

4.4 Bead assays and data analysis

Cells were sheared to truncate flagella by passing 1 mL of the washed cell suspension 120 times between 2 syringes equipped with 23-gauge needles and connected by 7-cm-long polyethylene tubing (0.58 mm inside diameter, no. 427411; Becton Dickinson, Franklin Lakes, NJ). The sheared cell suspension was centrifuged (2 min at 4000 g) and concentrated into 80 µL. We immobilized the cells on a glass coverslip coated with poly-L-lysine (0.01%, catalog No. P4707; Sigma) and allowed to stand for 4 min. Then, a 0.269% (w/v) solution of 1.0-µm-diameter polystyrene latex beads (2.69%, catalog No. 07310; Polysciences, Warrington, PA) was flowed into the chamber and incubated for another 3 min. The unattached beads were washed away with a flow of motility medium at 500 µL/min. The chamber was kept under a constant flow of fresh motility medium (100 µL/min) by a syringe pump during measurements.

The rotation of beads was observed by a Nikon Ti-E inverted phase-contrast microscope at a magnification of 40× and

recorded with a fast complementary metal-oxide semiconductor camera (Flare 2M360-CL, IO Industries) at 367.5 frames per second. Each video of bead rotation was converted into a binary time series of CW and CCW states. We defined T_i^{CW} and T_i^{CCW} as the durations of the *i*th CW and CCW intervals of the motor. The CW bias was calculated by

$$CW_{bias} = \sum_i^n T_i^{CW} / (T_i^{CCW} + T_i^{CW}),$$

where *n* is the number of intervals.

To determine the correlation time of the CCW sequences, we used serial correlation coefficients for the CCW interval lengths. Each motor was measured for 18 min. The binary time series of CW and CCW states was divided into several sections, each 800 s long. The MATLAB function “autocorr” was used to calculate the autocorrelation function for the array of CCW interval lengths for each 800-second data section. The relationship between the autocorrelation function and the number of CCW intervals was obtained.

For each time series, we performed 300 random shuffles and calculated the autocorrelation functions for these 300 reshuffled series. To determine whether the sequences in each lag (the number of preceding CCW intervals) were correlated, we used the Wilcoxon rank sum test (the “ranksum” MATLAB function) at a significance level of $P = 0.01$ compared to the reshuffled time series. We considered the first lag with nonzero correlation as the end of the correlation, obtaining the first unrelated CCW interval. We then obtained the correlated CCW interval number n_c and calculated the motor correlation time for each 800-second data section as

$$t_{correlation} = \sum_{i=1}^{n_c} CCW(i) + \sum_{i=1}^{n_c} CW(i) + \frac{CCW(n_c + 1)}{2},$$

where $CCW(i)$ and $CW(i)$ are the lengths of the *i*th CCW and CW intervals, respectively.

4.5 Simulation of bacterial chemotaxis

In the simulation, cells were treated as self-propelled particles that could swim smoothly (a run) with a constant speed of 25 µm/s under the effect of rotational diffusion (the rotational diffusion coefficient was $0.062 \text{ rad}^2/\text{s}^{[48]}$) or stop moving and choose a new swim direction (a tumble). The tumble angles θ obey the probability distribution^[48, 49]:

$$P(\theta) = 0.5(1 + \cos\theta) \sin\theta.$$

The swimming states are determined by the intracellular chemotactic signaling pathway. As the ligand concentration changed, the kinase activity of chemoreceptors was recalculated by Eq. (1). We used the parameters $K_{off} = 18.2 \text{ µmol/L}$, $K_{on} = 3 \text{ mmol/L}$, and $N=6$ for MeAsp. Then, the CheY-P concentration (Y_p) should also be renewed by $Y_p = 7.86a$. Finally, CheY-P binds to the motor and changes the CW bias (B) by Eq. (3). The switching rate of cellular motion from run to tumble was determined as $B/0.11 \text{ s}^{-1}$, while the switching rate from tumble to run was 5 s^{-1} . The adaptation of kinase activity was carried out by changing the methylation level of receptors, which was described by Eq. (2).

Cells started moving in a random direction from the origin of the coordinates. The time step was set to 0.01 s. We

simulated 2000 cells for 1200 s in an exponential MeAsp concentration profile $L(x) = 91 \exp(x/5000) \mu\text{mol/L}$, where x was in units of μm . k_r was changed from 10^{-5} s^{-1} to 1.0 s^{-1} , and k_b was set to $2k_r$.

Acknowledgements

This work was supported by the Natural Science Foundation of Anhui Province (2008085QA31).

Conflict of interest

The authors declare that they have no conflict of interest.

Biographies

Shujian Ren received her master's degree from the School of Physics, University of Science and Technology of China, under the supervision of Prof. Junhua Yuan and Prof. Rongjing Zhang.

Chi Zhang is an Associate Research Fellow at Hefei National Research Center for Physical Sciences at the Microscale, University of Science and Technology of China (USTC). He received his Ph.D. degree from the School of Physics, USTC, under the supervision of Prof. Junhua Yuan and Prof. Rongjing Zhang. His research mainly focuses on the chemotaxis and motion of bacteria in the biological physics field.

Rongjing Zhang is a Professor at the University of Science and Technology of China. She received her Ph.D. degree from the California Institute of Technology, USA. Her research mainly focuses on biofilm, bacterial motility and behavior, multi scale experimental measurement and characterization, and molecular motor in the biological physics field.

References

- [1] Armitage J P, Schmitt R. Bacterial chemotaxis: Rhodospirillum rubrum and Sinorhizobium meliloti—Variations on a theme? *Microbiology*, **1997**, *12*: 3671–3682.
- [2] Bren A, Eisenbach M. How signals are heard during bacterial chemotaxis: Protein-protein interactions in sensory signal propagation. *Journal of Bacteriology*, **2000**, *182*: 6865–6873.
- [3] Ud-Din A I M S, Roujeinikova A. Methyl-accepting chemotaxis proteins: A core sensing element in prokaryotes and Archaea. *Cellular and Molecular Life Sciences*, **2017**, *74*: 3293–3303.
- [4] Wadhams G H, Martin A C, Armitage J P. Identification and localization of a methyl-accepting chemotaxis protein in Rhodospirillum rubrum. *Molecular Microbiology*, **2000**, *36*: 1222–1233.
- [5] Falke J J, Hazelbauer G L. Transmembrane signaling in bacterial chemoreceptors. *Trends in Biochemical Sciences*, **2001**, *26*: 257–265.
- [6] Briegel A, Ladinsky M S, Oikonomou C, et al. Structure of bacterial cytoplasmic chemoreceptor arrays and implications for chemotactic signaling. *eLife*, **2014**, *3*: 02151.
- [7] Bi S, Lai L. Bacterial chemoreceptors and chemoeffectors. *Cellular and Molecular Life Sciences*, **2015**, *72*: 691–708.
- [8] Koler M, Peretz E, Aditya C, et al. Long-term positioning and polar preference of chemoreceptor clusters in *E. coli*. *Nature Communications*, **2018**, *9*: 4444.
- [9] Wadhams G H, Armitage J P. Making sense of it all: Bacterial chemotaxis. *Nature Reviews Molecular Cell Biology*, **2004**, *5*: 1024–1037.
- [10] Partridge J D, Nhu N T Q, Dufour Y S, et al. *Escherichia coli* remodels the chemotaxis pathway for swarming. *mBio*, **2019**, *10* (2): e00316-19.
- [11] Welch M, Oosawa K, Aizawa S, et al. Phosphorylation-dependent binding of a signal molecule to the flagellar switch of bacteria. *Proceedings of the National Academy of Sciences of the United States of America*, **1993**, *90*: 8787–8791.
- [12] Toker A S, MacNab R M. Distinct regions of bacterial flagellar switch protein FliM interact with FliG, FliN and CheY. *Journal of Molecular Biology*, **1997**, *273*: 623–634.
- [13] Chang Y, Zhang K, Carroll B L, et al. Molecular mechanism for rotational switching of the bacterial flagellar motor. *Nature Structural & Molecular Biology*, **2020**, *27*: 1041–1047.
- [14] Duke T A J, Bray D. Heightened sensitivity of a lattice of membrane receptors. *Proceedings of the National Academy of Sciences of the United States of America*, **1999**, *96*: 10104–10108.
- [15] Ames P, Studdert C A, Reiser R H, et al. Collaborative signaling by mixed chemoreceptor teams in *Escherichia coli*. *Proceedings of the National Academy of Sciences of the United States of America*, **2002**, *99*: 7060–7065.
- [16] Sourjik V, Berg H C. Receptor sensitivity in bacterial chemotaxis. *Proceedings of the National Academy of Sciences of the United States of America*, **2002**, *99*: 123–127.
- [17] Lamanna A C, Gestwicki J E, Strong L E, et al. Conserved amplification of chemotactic responses through chemoreceptor interactions. *Journal of Bacteriology*, **2002**, *184*: 4981–4987.
- [18] Barkai N, Leibler S. Robustness in simple biochemical networks. *Nature*, **1997**, *387*: 913–917.
- [19] Silverman M, Simon M. Chemotaxis in *Escherichia coli*: Methylation of the gene products. *Proceedings of the National Academy of Sciences of the United States of America*, **1977**, *74*: 3317–3321.
- [20] Antommattei F M, Munzner J B, Weis R M. Ligand-specific activation of *Escherichia coli* chemoreceptor transmethylation. *Journal of Bacteriology*, **2004**, *186*: 7556–7563.
- [21] Lan G, Schulmeister S, Sourjik V, et al. Adapt locally and act globally: Strategy to maintain high chemoreceptor sensitivity in complex environments. *Molecular Systems Biology*, **2011**, *7*: 475.
- [22] Paulick A, Jakovljevic V, Zhang S, et al. Mechanism of bidirectional thermotaxis in *Escherichia coli*. *eLife*, **2017**, *6*: 26607.
- [23] Meir Y, Jakovljevic V, Oleksiuk O, et al. Precision and kinetics of adaptation in bacterial chemotaxis. *Biophysical Journal*, **2010**, *99*: 2766–2774.
- [24] Micali G, Endres R G. Bacterial chemotaxis: Information processing, thermodynamics, and behavior. *Current Opinion in Microbiology*, **2016**, *30*: 8–15.
- [25] Kim C, Jackson M, Lux R, et al. Determinants of chemotactic signal amplification in *Escherichia coli*. *Journal of Molecular Biology*, **2001**, *307*: 119–135.
- [26] Hansen C H, Endres R G, Wingreen N S. Chemotaxis in *Escherichia coli*: A molecular model for robust precise adaptation. *PLoS Computational Biology*, **2008**, *4*: e1.
- [27] Li M, Hazelbauer G L. Adaptational assistance in clusters of bacterial chemoreceptors. *Molecular Microbiology*, **2005**, *56*: 1617–1626.
- [28] Endres R G, Wingreen N S. Precise adaptation in bacterial chemotaxis through “assistance neighborhoods”. *Proceedings of the National Academy of Sciences of the United States of America*, **2006**, *103*: 13040–13044.
- [29] Mello B A, Tu Y. Perfect and near-perfect adaptation in a model of bacterial chemotaxis. *Biophysical Journal*, **2003**, *84*: 2943–2956.
- [30] Keymer J E, Endres R G, Skoge M, et al. Chemosensing in *Escherichia coli*: Two regimes of two-state receptors. *Proceedings of the National Academy of Sciences of the United States of America*, **2006**, *103*: 1786–1791.
- [31] Dzinic S H, Shukla M, Mandija I, et al. Variable length tandem repeat polyglutamine sequences in the flexible tether region of the Tsr chemotaxis receptor of *Escherichia coli*. *Microbiology*, **2008**, *154*: 2380–2386.

- [32] Mello B A, Tu Y. Quantitative modeling of sensitivity in bacterial chemotaxis: The role of coupling among different chemoreceptor species. *Proceedings of the National Academy of Sciences of the United States of America*, **2003**, *100*: 8223–8228.
- [33] Lan G, Sartori P, Neumann S, et al. The energy-speed-accuracy trade-off in sensory adaptation. *Nature Physics*, **2012**, *8*: 422–428.
- [34] Sourjik V, Vaknin A, Shimizu T S, et al. [17]-in vivo measurement by FRET of pathway activity in bacterial chemotaxis. In: Simon M I, Crane B R, Crane A, editors. *Methods in Enzymology: Two-Component Signaling Systems, Part B*. Amsterdam: Elsevier, **2007**: 365–391.
- [35] McEvoy M M, Bren A, Eisenbach M, et al. Identification of the binding interfaces on CheY for two of its targets the phosphatase CheZ and the flagellar switch protein FliM. *Journal of Molecular Biology*, **1999**, *289*: 1423–1433.
- [36] Zhang C, He R, Zhang R, et al. Motor adaptive remodeling speeds up bacterial chemotactic adaptation. *Biophysical Journal*, **2018**, *114*: 1225–1231.
- [37] Liu X, Zhang C, Zhang R, et al. The effect of the second messenger c-di-GMP on bacterial chemotaxis in *Escherichia coli*. *Applied and Environmental Microbiology*, **2022**, *88*: e0037322.
- [38] Tu Y, Shimizu T S, Berg H C. Modeling the chemotactic response of *Escherichia coli* to time-varying stimuli. *Proceedings of the National Academy of Sciences of the United States of America*, **2008**, *105*: 14855–14860.
- [39] Jiang L, Ouyang Q, Tu Y. Quantitative modeling of *Escherichia coli* chemotactic motion in environments varying in space and time. *PLoS Computational Biology*, **2010**, *6*: e1000735.
- [40] Monod J, Wyman J, Changeux J P. On the nature of allosteric transitions: A plausible model. *Journal of Molecular Biology*, **1965**, *12*: 88–118.
- [41] Vladimirov N, Løvdok L, Lebedz D, et al. Dependence of bacterial chemotaxis on gradient shape and adaptation rate. *PLoS Computational Biology*, **2008**, *4*: e1000242.
- [42] Tian M, Zhang C, Zhang R, et al. Collective motion enhances chemotaxis in a two-dimensional bacterial swarm. *Biophysical Journal*, **2021**, *120*: 1615–1624.
- [43] Tu Y, Grinstein G. How white noise generates power-law switching in bacterial flagellar motors. *Physical Review Letters*, **2005**, *94*: 208101.
- [44] Park H, Pontius W, Guet C C, et al. Interdependence of behavioural variability and response to small stimuli in bacteria. *Nature*, **2010**, *468*: 819–823.
- [45] Zhang C, Zhang R, Yuan J. Growth-dependent behavioral difference in bacterial chemotaxis. *Physical Review E*, **2017**, *95*: 062404.
- [46] Cluzel P, Surette M, Leibler S. An ultrasensitive bacterial motor revealed by monitoring signaling proteins in single cells. *Science*, **2000**, *287*: 1652–1655.
- [47] He R, Zhang R, Yuan J. Noise-induced increase of sensitivity in bacterial chemotaxis. *Biophysical Journal*, **2016**, *111*: 430–437.
- [48] Vladimirov N, Lebedz D, Sourjik V. Predicted auxiliary navigation mechanism of peritrichously flagellated chemotactic bacteria. *PLoS Computational Biology*, **2010**, *6*: e1000717.
- [49] Berg H C, Brown D A. Chemotaxis in *Escherichia coli* analysed by three-dimensional tracking. *Nature*, **1972**, *239*: 500–504.